Published in : Materials Research (2026), vol. 194, pp. 113793
DOI: 10.1016/j.materresbull.2025.113793
Status : Postprint (Author's version)

SUB-TERAHERTZ ABSORPTION SHIELDING PERFORMANCES OF POLYURETHANE - CARBON NANOTUBES COMPOSITE FOAMS

Ahmad Mamoun Khamis [a,], Laetitia Urbanczyk [b], Christophe Detrembleur [b,c], Isabelle Huynen [a]

[a] *ICTEAM Institute, Université Catholique de Louvain, Louvain-la-Neuve, 1348 Belgium*
[b] *Center for Education and Research on Macromolecules (CERM), CESAM Research Unit, University of Liege, Sart-Tilman B6a, 4000 Liege, Belgium*
[c] *WEL Research Institute, Avenue Pasteur 6, 1300 Wavre, Belgium*

Abstract

This study presents a novel investigation of the impact of multiwalled carbon nanotube (CNT) on the microstructure and electromagnetic shielding properties of polyurethane (PU) foams across an exceptional ultra-wideband frequency range, from 5.85 GHz to 330 GHz. The microstructure results show that the CNT formed an interconnected and well-distributed network on the PU surface. In addition, increasing CNT content from 1 wt.% to 11.2 wt.% significantly enhanced the total shielding effectiveness (SE_T) by approximately four times over the whole frequency range. The absorption is identified as the main mechanism contributing to the SE_T performance of our 2.4 mm-thick foamed composite samples, representing >98 % of the SE_T above 40 GHz and up to 330 GHz. Hence, the corresponding absorption level achieved in this range is 13 – 45 dB. Our samples exhibit significant potential for electromagnetic interference shielding applications since they meet the standard commercial requirements.

Keywords : Electromagnetic shielding effectiveness Absorption, Carbon nanotubes, Polyurethane foam, Submillimeter wave

1. Introduction

Electromagnetic interference (EMI) has recently gained attention because of the rapid developments in electronic products and technology. EMI poses a risk to human lives and the economy due to the interference with the normal operations of circuits, components, communications, and electronic equipment [1–4]. Therefore, shielding the electrical apparatuses over a wide range of frequencies is crucial to ensure their proper function. Metals are traditionally used for this purpose; however, metals have drawbacks such as poor corrosion resistance and large weight [5–7]. To overcome these drawbacks, many researchers have been focusing on polymer-based materials due to their multiple

advantages such as corrosion resistance, low weight, flexibility, and low cost. Nevertheless, most polymers have insulating electrical characteristics, making them poor shielding materials. Therefore, conductive nanoparticles are used as fillers to enhance the electromagnetic (EM) shielding performance, especially the absorption which is highly preferred in many applications [8,9]. Recently, anchored C/Co and C/Co_3Se_4 cobalt-based nanoplates were prepared for the purpose of designing and regulating their microscopic electron behavior and macroscopic electromagnetic response. Such nanoplates can effectively absorb and convert unwanted gigahertz EM radiation into used heat energy [10]. Lei et al. also prepared a (CoFeNiCuMn)O composite supported with reduced graphene oxide, synthesized using plasma process, for EM absorption applications [11]. High entropy (HE) materials have been extensively investigated for EM wave absorption due to the unique HE effect, hysteresis diffusion, lattice distortion effect, and synergistic effects, which are expected to meet the requirements of a wide range of applications [12]. In addition, a multifunctional magnetic CNTs heterodimensional structure was assembled through interface and defect engineering, for improving the EMI shielding performance [13].

Carbon foam also emerged as an attractive candidate in EMI shielding applications due to its low density, protection against shocks, resistance to chemical corrosion and to high temperature [14]. In addition, polyurethane foams have recently started to replace plastics and metals in many engineering applications by combining the flexibility of rubber with the durability and hardness of metal [15]. Many researchers have studied the effects of multiwalled carbon nanotubes on the EM properties of the polyurethane but they only focused on the following frequency ranges: $10^1 – 10^6$ Hz [16], 8.2 - 12.4 GHz [17–20], 1–18 GHz [21], and 5 – 50 GHz [22]. This indicates there is no previous research that has conducted such studies in a broad frequency range, leading to a lack of information reported in literature. Therefore, our study fills a gap in literature by investigating the EM shielding properties of CNT-PU composites in the 5.85 – 330 GHz frequency range. This investigation helps in extending the usage of CNT-PU samples in EMI shielding applications. The CNT-foam samples can be fabricated using two main methods. In the first one which is called the bottom-up method, the CNTs are directly dispersed in the polymer matrix, followed by the foaming process as described in [23,24]. In the second method, the CNTs are deposited onto a ready-made foam sample by dip-coating process [25–27].

The terahertz (THz) waves are electromagnetic waves that have a wavelength and frequency of 30 μm to 1 mm and 0.3 to 10 THz in a vacuum, respectively. Waves generally have a high penetration capability through non-polar materials, while they have significant absorption properties when interacting with polar materials. On the other hand, the sub-terahertz waves, with wavelengths and frequencies ranging from 1 to 10 mm and 0.03 to 0.3 THz, respectively, share similar properties with THz waves but offer superior transmission properties [28]. The sub-THz band has started to be used in various applications such as 5 G networks and it is also paving the way for 6 G, which will use the carrier frequencies higher than millimeter to provide point-to-point communication, and the 100 – 300 GHz frequency range is considered the first effective window [29]. This rapid growth of millimeter-wave technologies has caused major difficulties in controlling the EMI and maintaining stable operation of electronic devices [30]. To address this urgent need, it is crucial to investigate the capabilities of EMI shielding materials in the millimeter wave frequency range.

The carbon-based foams are relatively new materials for the THz absorber applications. The inner structure is the main feature of these materials. The void spaces contained in the pore structure behave like cavities where the THz waves go through multiple reflections [31] and get absorbed by the material. Even though extensive studies have been conducted on the EM wave absorption of carbon foam materials in the microwave range, fewer studies have been recorded in the THz range [32]. The carbon nanotubes were used in the sub-THz range of frequencies to conduct studies for several applications, such as antenna [33], thin films deposited on fused quartz [34], optically tunable THz devices [35], and photothermal devices [36]. Our study extends the applications of CNT to the EMI shielding field in the sub-THz range. In general, the characterizations in the THz frequency range were conducted using a time domain spectroscopy system [37–40] or a network analyzer equipped platform with a pair of frequency extenders [41,42].

This study presents a novel perspective on investigating EM shielding and absorption performance of CNT-PU samples in frequency bands ranging from 5.85 to 330 GHz. The impact of CNT content on the microstructure of PU surface is also presented. To the best of our knowledge, it is the first time that CNT-PU foam samples are characterized in an ultra-wide frequency range using frequency extenders (W-band, D-band, and J-band) and different waveguides to investigate the EMI shielding effectiveness and absorption from 5.85 GHz up to 330 GHz frequency range. An experimental analysis of absorbed, reflected, transmitted power, and shielding effectiveness is proposed and is supported by an SEM analysis of the morphology of the fabricated nanocomposite foams.

2. Experimental section

This section presents the following subjects: the raw materials used to fabricate the CNT-PU samples, the fabrication process of the samples, the microstructure and electromagnetic characterization, and the equations used to evaluate the shielding performance.

2.1. MATERIALS

The CNT-PU samples were prepared using the following materials: open-cell polyurethane foam (SiPLA SA, Wavre, Belgium) with a net density of 54 kg/m^3 and an average pore diameter of 0.46 mm, and AQUACYL™ AQ0303 multiwall carbon nanotubes waterborne dispersion (Nanocyl SA, Sambreville, Belgium).

2.2. SYNTHESIS OF CNT-PU SAMPLES

The CNT-PU foam samples were prepared using the dip-coating method. The CNT solution was prepared by diluting the commercial CNT/water masterbatch Aquacyl 0303 with the appropriate amount of distilled water. The dilution factors used were 1/4, 1/10, 1/20, and 1/40 for a total volume of 1200 ml. The PU foam was then dipped in the diluted CNT solution for 24 h. The foam was immersed by applying weight (1 kg) on the whole surface of the foam and squeezed five times in the first hour to

promote liquid penetration in the foam. Then, the foam samples were removed and dried in a vacuum oven at 70 °C for 1 day. The amount of CNT incorporated is deduced from the weight difference of the foam before and after the dipping process. This fabrication process led to four CNT-PU samples with different CNT contents (1 wt. %, 2.3 wt. %, 6 wt. %, and 11.2 wt. %). The prepared samples shared the same surface dimensions (16 cm x 16 cm) and a thickness of 2 cm. Finally, the sample dimensions were reduced for EM characterization to 7 cm × 7 cm × 2.4 mm using a cutter and 3D-printed holder.

2.3. CHARACTERIZATIONS

The microstructure and morphology of CNT-PU samples were examined using the scanning electron microscopy (SEM). An Anritsu vector network analyzer (VNA) and Keysight PNA were used to characterize the scattering parameters of CNT-PU samples in the 5.85 – 40 GHz and 40 – 330 GHz frequency ranges, respectively. The calculations of EM absorption and shielding parameters are introduced in Eqs. (1) – (7).

2.3.1. SCANNING ELECTRON MICROSCOPY

The SEM is an essential tool for investigating nanomaterials since it provides the observation of structure, shape, and size [43]. A JEOL 7600F SEM, operating at 15 keV, was used to investigate the dispersion of CNT in the CNT-PU samples. The specimens were mounted on stubs and coated with a 12 nm gold layer using the Cressington sputter 208HR to create a thin conductive layer to minimize degradation and drift due to thermal expansion. Finally, the stubs were placed inside the SEM chamber for analysis.

2.3.2. EM MEASUREMENTS IN THE 5.85 – 60 GHZ FREQUENCY RANGE

The measurements of scattering parameters (reflection and transmission coefficients S_{11} and S_{21}) were performed in the 5.85 - 40 GHz frequency range using an Anritsu VNA (MS4644B). Meanwhile, a Keysight PNA (N5227B) network analyzer was used for measurements from 40 to 60 GHz. The VNA was calibrated using a Thru-Reflect-Line (TRL) method for 801 points at room temperature for each frequency range. Then, the material under test (MUT) was carefully placed between the waveguide flanges to avoid air gaps, and the measurements were conducted for each frequency range to obtain the reflection and transmission coefficients corresponding to the reflection of EM signal at the input of the sample and transmission through it, respectively. This so-called “flange method” [44] offers many advantages: it is non-destructive, adaptable to the material under test (MUT) thickness, and does not require fabricating the MUT with specific dimensions. Hence, a single MUT with a large surface can be characterized across a wide range of frequencies.

2.3.3. EM MEASUREMENTS IN THE 75 – 330 GHZ FREQUENCY RANGE

A Keysight PNA (N5227B) network analyzer with N5292A Millimeter Test Set connected to the frequency extenders of W-band (N5295AX03, Keysight), D-band (VDI, Virginia Diodes), and J-band (VDI, Virginia Diodes) was used to conduct the measurements. The frequency extenders of W-band, D-band, and J-band cover the following frequency ranges 75 – 110 GHz, 110 – 170 GHz, and 220 – 330 GHz,

respectively. The calibration for W-band was conducted using the 85058B standard calibration kit (Keysight, 1.85 mm) which includes LB Load (50788), Open (51330), Short 1 (51830), Short 2 (50685), Short 3 (50681), Short 4 (50673), and Line. The calibration kits for D and J bands were WR6.5 (VDI) and WR3.4 (VDI). The D and J bands shared the same calibration procedures of the Thru-Reflect-Line (TRL) [45] for 201 points at room temperature. Thru was conducted by directly connecting the waveguide flanges, Reflect was conducted using SCR3 Short (15–175), and Line was conducted using a quarter-wave Shim. Two 3D-printed holders were designed and fabricated at the WELCOME facility of UCLouvain to enhance the measurement accuracy of D and J bands frequency extenders. Such holders preserve perfect alignment of frequency extenders to ensure the maximum transmission power from the input to the output port [42]. After performing and validating the calibration, the measurements were conducted by carefully inserting the MUT between the flanges. Finally, Microsoft Excel combined the reflection and transmission results obtained using the PNA and VNA systems in a single curve for each sample.

2.4. OBTENTION OF ELECTROMAGNETIC ABSORPTION AND SHIELDING EFFECTIVENESS

The fraction of EM absorbed power (A) inside our CNT-PU samples is evaluated using the following formula:

$$A = 1 - R - T \quad (1)$$

Where the fractions of reflected power (R) and transmitted power (T) are evaluated using the following two equations involving the S-parameters (S_{11} and S_{21}) measured by a VNA [46]:

$$R = |S_{11}|^2 \quad (2)$$

$$T = |S_{21}|^2 \quad (3)$$

In the next sections, the fractions of R, T and A will be represented in percent; 100 x R, 100 x T, and 100 x A, respectively.

The total shielding effectiveness (SE_T) of CNT-PU samples is defined as a function of T as follows:

$$SE_T = -10 \times \log_{10}(T) \quad (4)$$

Where T was calculated using Eq. (3). The contribution of reflection loss and absorption loss to the total shielding was calculated using the following equations [27]:

$$SE_R = -10\log(1 - R) \quad (5)$$

$$SE_A = -10\log\left(\frac{T}{1-R}\right) \quad (6)$$

The SE_T is a combination of the three following mechanisms [47]:

$$SE_T = SE_R + SE_{MR} + SE_A \quad (7)$$

Where SE_R, SE_{MR}, and SE_A represent the shielding effectiveness due to reflection, multiple internal reflections, and absorption, respectively. The SE_{MR} can be neglected when the SE_T is greater than 10 dB

[27]. The increase in shielding efficiency in decibel (dB), corresponds to an increase in energy consumption in the shielding material [48].

It is worth noting that Eq. (7) is widely used in literature to calculate the SE_T [24,27]. In our study, Eq. (4) was used to calculate the SE_T. Eqs. (4) and (7) give the same results because the impact of SE_{MR} is negligible.

3. Results and discussions

3.1. MORPHOLOGY ANALYSIS

The morphology of CNT-PU composites was characterized using the SEM. The images of pure PU in Fig. 1 (a and b) show a relatively smooth skeleton. This observation is in line with foam morphologies reported in previous studies [49,50]. The PU foam has an open-cell structure with pores ranging from 108 to 843 µm, as shown in Fig. 1a. The apparent CNT diameter ($D_{apparent}$) sizes presented in Fig. 1*g* show the values of 30.9 nm and 25.5 nm. However, these numbers do not represent the real values of CNT diameters because of a gold coating layer of thickness L = 12 nm is present on both sides of the diameter. Therefore, the real value (D_{real}) of CNT diameter was calculated using the following formula:

$$D_{real} = D_{apparent} - 2L \quad (8)$$

The real CNT diameter ranges from 6.9 to 1.5 nm. Similarly, the real length of the CNT ranges from 295 nm to 445 nm, which is calculated by subtracting 24 nm from the values presented in Fig. 1i. However, the length values mentioned only represent the apparent side of CNT, not the whole length of CNT. The cracks visible on the surface of PU foam samples were due to the gold coating. The CNTs are visible and evenly distributed throughout the sample with no accumulation. This observation is per the study [51], which reported that CNTs with a large ratio of length to diameter tend to tangle with each other to form the conductive networks.

The entangled structure presented in the images of CNT-PU samples shows that the CNTs are intertwined together to form interconnected networks. Furthermore, the PU surface, shown in Fig. 1 (a and b), is not detected in all CNT-PU specimens (Fig. 1c-j), indicating that the CNT networks covered the entire PU surface. The SEM images also show that increasing the CNT content does not significantly impact the nanostructure of CNT-PU samples because the images of Fig. 1 (d, f, h, and i), which share the same magnification scale of 35 K, display similar CNT networks. This could be due to the tiny scale of CNT, which was evenly dispersed on the PU surface, making it difficult to visually distinguish the impact of increasing CNT content on the interconnected networks. In other words, the visible surface density of CNT-PU samples seems unchanged with increasing CNT content because SEM technique only examines the MUT surface covered by CNT. This technique cannot examine the thickness of CNT layer that normally increases with increasing CNT loading in the samples. The CNT successfully formed an interconnected network in the 1 wt. % CNT sample which had the lowest CNT content. Therefore, increasing the content of CNT by>1 wt. % does not produce an observable change in the microstructure

since it is only possible to examine the specimen surface not the thickness of the CNT layer in each sample.

3.2. ELECTROMAGNETIC BEHAVIOR OF CNT-PU SAMPLES

Eq. (1) reveals that obtaining good absorption implies minimizing the fractions of reflected power R and transmitted power T. The behavior of R, T, and A is discussed in the following subSections 3.2.1, 3.2.2, and 3.2.3, respectively. From the discussion, it will be concluded that EM absorption is the main mechanism involved in the EMI shielding achieved by our CNT-PU composites. The two factors that influenced the EM absorption are as follows:

1. The CNT which has a high electrical conductivity [52].
2. The PU foam which has electrical insulation properties [53].

3.2.1. REFLECTED POWER (R)

The fraction of reflected power, presented in Table 1 and Fig. 2, was extracted from measurements of CNT-PU samples using Eq. (2). The 11.2 wt. % CNT sample exhibited the highest R in the 5.85 – 40 GHz frequency range. This behavior could be attributed to the high content of CNT which has high electrical conductivity whereby the electrons migrates to form a conductive current in the presence of EM field [54].

The reflected power decreased with increasing CNT concentrations above 40 GHz, this decrement can be associated with the behavior of the absorption, which will be discussed in SubSection 3.2.3. This is also confirmed in literature that the loss in reflection is an important parameter in evaluating the absorption performance of EM-absorbing materials [55]. This is because the transmitted and reflected waves significantly decrease with greatly enhanced absorption [56].

Overall, the behavior of R is induced by the foamed structure of the material under scope. The air filling factor of our foams exceeds 90 %, which combined with the nominal value of the dielectric constant of PU lower than 3.6 [57], yields a low value of dielectric constant of the composite foam, around 1.26 thus close to air and lowering the reflection. This partly explains that the reflected power remains below 10 % above 40 GHz. Moreover, the reduction of reflection can also be favored by the presence of percolative conductive CNT network that, above a threshold frequency (around 40 GHz in our case), contributes to favor the absorption of the signal into the foam.

3.2.2. FRACTION OF TRANSMITTED POWER (T) AND ASSOCIATED TOTAL SHIELDING EFFECTIVENESS SE_T

The fraction of transmitted power (T) is shown in Fig. 3. Increasing the CNT content induces a decrease in the transmitted power over the whole frequency range. This is consistent with the conductive nature of the CNT; increasing the conductive content also increases the ohmic losses in the samples, hence their capacity to attenuate and block the EM wave. A low transmitted power is associated with a high SE_T according to Eq. (4).

The shielding is mainly dependent on absorption because the reflection R of CNT-PU composites remains below 10 % above 40 GHz as presented in Fig. 2. In general, higher absorption and reflection lead to lower transmission and thus higher SE_T as presented in Figs. 3 and 4, respectively. In our case, as reflection is not significant, the high SE_T is mainly due to absorption. The variation in SE_T among the samples is relatively small in low frequencies and significantly grows with increasing frequency. It is attributed to the capacitive coupling occurring between CNT at high frequency, responsible for the formation of an efficient percolative conductive network at microwaves and sub-THz frequencies [58]. For each CNT content, the SE_T is clearly maximum in the 220 – 330 GHz frequency range and is influenced by the CNT content, as summarized in Table 2and shown in Fig. 4. This performance will be compared to state-of-the-art in SubSection 3.2.4.

It can already be noted that the SE_T of 11.2 wt. % and 6 wt. % samples reaches the threshold of 20 dB, which is the targeted value for commercial absorbers, above 26.5 GHz and 110 GHz, respectively.

3.2.3. EM ABSORPTION OF POWER

The EM absorption represented the energy dissipation resulting from the interaction between EM signals and the absorber [48]. When EM signals pass through conductive composite materials, EM absorption occurs and converts EM energy into heat energy due to ohmic loss. The origin of ohmic loss can be the energy dissipation by mobile charge carriers through electrical conduction, hopping, and tunneling. Under an external EM field, the free electrons migrate and hop through conductive networks [56] constructed by CNT. Therefore, the conductivity of the composites is determined by electronic transport. The hopping electrons can jump across the interface between CNTs, and this hopping mechanism can improve the micro-current in the CNT networks when the CNT filling content is sufficient [59]. Gong et al. [60] found that increasing the CNT content increases the number of dissipating charge carriers, causing higher ohmic loss. The fraction of absorbed power, calculated using Eq. (1), is presented in Fig. 5 and Table 3.

Ohmic loss is dependent on the skin depth, which decreases with increasing frequency. Skin depth (δ) is the depth from the surface where the electric field incident on the material has diminished to 1/e of its value at the surface [61]. The skin depth is calculated using the following formula [62]:

$$\delta = \frac{1}{\sqrt{\pi f \mu \sigma}} \quad (9)$$

Where σ and μ represent the material's conductivity and permeability, respectively, and f is the frequency. Based on Eq. (9), the skin depth is around seven times smaller at 330 GHz compared to 5.85 GHz, which means that the power (current) density at 330 GHz is greater compared to 5.85 GHz. This will lead to a higher ohmic loss (joule heating) per volume unit when increasing the frequency, because the relationship between the ohmic loss and power density is directly proportional. Hence, the absorption will increase with increasing frequency since higher ohmic loss at higher frequencies is associated with higher absorption. The interconnected and well distributed CNTs, discussed in Section 3.1, formed a conductive network in the CNT-PU composites on the nanoscale. The electron transport in the CNT networks could be explained as a series of circuit model where the hopping and migrating transports take place in parallel [59]. Such transport is influenced by the CNT content. Therefore, the

currents induced by the EM signal in the CNTs, uniformly covering the whole surfaces of CNT-PU composites, might lead to a higher absorption.

Apart from conduction losses associated with the CNTs present in the dielectric PU matrix, there are four types of polarization possible in dielectric materials: electronic, ionic, dipole-oriented, and interfacial (space charge). The total polarizability in a dielectric material is the sum of these four contributions [63]. The electronic polarization occurs due to the displacement of the outer electron clouds with respect to the inner positive atomic cores [64]. This polarization can be neglected in this study since it takes place in the optical frequency range around 10E15 Hz, and the frequencies where the electric field oscillates in our study are too low to stimulate the electronic polarization. The interfacial polarization occurs due to the accumulation of charges at the interfaces between CNT nanofillers and the PU matrix. This type of polarization is also ignored in this study because it takes place in low-frequency ranges around 10 kHz [65]. Additionally, ionic polarization does not occur in the CNT-PU composites because both CNT and PU have covalent bonds. Dipole polarization might be dominant in our study because the urethane [-NH–CO–O-] group, which is the main building block of polyurethanes [66], exhibits a dipole moment. The dipolar polarizability describes the second-order response of a system to an external electric field perturbation [67]. However, the dipoles start to lag behind the field as the frequency increases, leading to a lower absorption [68].

Both CNTs and PU contribute to the overall absorption of CNT-PU composites, but the contribution of CNT is higher than that of PU. This is because the PU is an electrically insulating material compared to CNT, which is a conductive material and has more potential to dissipate the EM power through ohmic loss. Such materials are highly recommended in EMI shielding applications because materials with high absorption capabilities combined with low reflectivity reduce the risk of dispersing spurious signals into the environment via multiple reflections [69].

Indeed, the absorption cannot take place inside the sample if the EM signals are totally reflected at its surface. Highly conductive materials, such as copper, have high reflectivity and limited absorption potential. Therefore, highly conductive materials use the first shielding mechanism (reflection) to suppress the EM waves in EMI shielding applications. In this study, the CNT-PU composites greatly rely on the absorption mechanism to attenuate the EM energy, also reducing the EMI caused by signals reflected to the surrounding environment.

3.2.4. SUMMARY OF SHIELDING PERFORMANCE AND COMPARISON WITH STATE-OF-THE ART

As discussed in the previous sections, the SE_T performance in our sample is mainly due to absorption. This is illustrated by the bar charts shown in Fig. 6 where the SE_R and SE_A values are obtained from Eqs. (5) and (6), respectively. Whatever the frequency and CNT concentration, the reflection R is not significant and does not influence the total shielding performance SE_T, which is close to the shielding achieved by absorption.

Tables 4 and 5 present a comparison of SE_T values between our study and recent studies in the literature at 9 GHz and in the sub-THz range, respectively. The specific shielding effectiveness (SSE) of the samples was calculated using the following formula:

$$SSE\ (dB/mm)\ = \frac{SE_T\ (dB)}{Thickness\ (mm)} \quad (10)$$

The SSE normalizes the shielding effectiveness to the thickness of the sample because it is confirmed in the literature that the thickness has a significant impact on the SE_T [70–72]. Normalizing to the thickness allows an independent comparison with performance from the literature, since for materials that are mostly absorbent, SE_A and SE_T are directly proportional to the thickness. Our material is mainly absorbent since SE_R is negligible according to Fig. 6. However, the SSE formula does not consider the filler percentage, which may lead to misleading comparisons. Therefore, we based our comparison on the β factor which considers the sample's thickness and CNT's percentage as expressed in the following equation.

$$\beta\ = \frac{SSE}{CNT\%} \quad (11)$$

Our CNT-PU composites exhibit the highest β factor compared to the corresponding values previously reported in the literature as presented in Table 4. Moreover, this study investigated the impact of CNT on PU foam matrix over a wide range of frequencies, paving the way for implementing CNT-PU composites in the SHF and millimeter wave EMI shielding applications.

In conclusion, the 11.2 wt. % CNT sample with 2.4 mm thickness meets the standard target values for commercial EMI shielding materials, which is 20 dB [73], above 26.5 GHz. Additionally, the SE_T performance can be significantly enhanced by increasing the thickness since the sample's thickness is directly proportional to the absorption loss [74].

Contrary to Table 4, the comparison presented in Table 5 does not include studies on CNT-PU composites due to the lack of related studies in the literature in the sub-THz. This gap also reflects the importance of investigating the shielding properties of CNT-PU composites at these frequencies. It is worth noting that some reported data in Table 5 shows higher SSE values compared to our results due to the following reasons: 1- The studies were conducted in the 0.5 – 3 THz frequency range and thus higher frequencies naturally caused higher SSE. 2- High content of filler was used in the composite. Hence, to the best of our knowledge, our presented samples are superior to previously published sub-THz composites, especially when taking into account the balance between the sample thickness, frequency range, filler percentage, and SE_T.

4. Conclusion

Four different CNT-PU foam samples were successfully fabricated by dip-coating, and their EM shielding and absorption properties were investigated across a broad frequency range of 5.85 – 330 GHz. The EM characterization across such a broad frequency range represents a key novelty of our study. Increasing the CNT content significantly influenced the absorption and SE_T performance of the samples at higher frequencies. The SEM images of CNT-PU samples showed that the CNT formed an interconnected and conductive network covering the entire surface of the PU foam. The prepared samples conform to the industrial requirements of EMI shielding materials. Notably, the 11.2 wt. %

sample achieved an SE_T between 20 dB and 45.3 dB in the 26.5 – 330 GHz frequency range. The contribution of the SE_R to the SE_T of 2.3 wt. %, 6 wt. % CNT and 11.2 % wt. % samples was <2 % while the contribution of SE_A was higher than 98 % in the 50 – 330 GHz frequency range. Therefore, the absorption was the main mechanism contributing to the SE_T due to the high absorption capabilities of CNT across the studied frequency range. Future work could focus on investigating the shielding effectiveness of CNT-PU samples in the 0.3 - 1 THz frequency range. Our study could also be re-conducted using different fillers and foam samples. For example, graphene oxides and ferrite nanoparticles could be used as fillers to enhance the SE_T and absorption performance of foam composites in future research.

Funding

This work was performed in the frame of the UP_Plastics project co- funded by the European Union and the Walloon Region as part of the FEDER 2021–2027 Program. The acquisition of the J–band measuring equipment was funded by the FNRS convention no U.N046.22, “On- wafer measurement of electromagnetic phenomena in materials, devices and circuits in $_D$-band (110–170 GHz)”.

CRediT authorship contribution statement

Ahmad Mamoun Khamis: Writing – review & editing, Writing – original draft, Investigation, Formal analysis, Data curation. **Laetitia Urbanczyk:** Writing – review & editing, Methodology, Investigation, Conceptualization. **Christophe Detrembleur:** Writing – review & editing, Supervision, Resources, Project administration, Methodology, Funding acquisition. **Isabelle Huynen:** Writing – review & editing, Writing – original draft, Supervision, Resources, Project administration, Funding acquisition, Formal analysis.

Declaration of competing interest

The authors declare that they have no known competing financial interests or personal relationships that could have appeared to influence the work reported in this paper.

Acknowledgments

The authors thank Pascal Simon and Benoît Hubert from the Welcome technological platform of UCLouvain for their great support in the measurements of CNT-PU samples. Benoît Hubert designed and fabricated the 3D-printed holders of D and J bands frequency extenders.

The authors also thank Delphine Magnin from IMCN of UCLouvain for conducting SEM characterization. The works of I. Huynen and C. Detrembleur as Research Directors are funded by the National Fund for Scientific Research (FNRS, Belgium).

Data availability

Data will be made available on request.

Tables

Table 1 *Fraction of reflected power of CNT-PU samples at selected frequencies.*

CNT wt. %	R (%)						
	5.85 GHz	20 GHz	50 GHz	90 GHz	140 GHz	220 GHz	330 GHz
1	9.0	2.2	4.5	5.0	2.2	7.7	4.0
2.3	19.3	6.9	1.0	2.4	1.8	1.1	1.2
6	30.8	9.5	0.9	1.0	0.3	3.5	3.0
11.2	56.7	23.9	1.8	1.4	1.0	1.9	1.4

Table 2 *SE_T (dB) of CNT-PU samples at selected frequencies.*

CNT wt. %	SE_T (dB)						
	5.85 GHz	20 GHz	50 GHz	90 GHz	140 GHz	220 GHz	330 GHz
1	4.4	4.3	5.8	13.4	12.0	11.8	13.3
2.3	8.2	11.9	14.1	14.4	15.7	16.0	16.6
6	12.8	14.9	17.1	19.0	23.6	25.2	25.9
11.2	16.9	18.1	23.9	28.2	34.6	41.3	45.3

Table 3. *Absorption of CNT-PU samples at selected frequencies.*

CNT wt. %	A (%)						
	5.85 GHz	20 GHz	50 GHz	90 GHz	140 GHz	220 GHz	330 GHz
1	54.7	60.8	69.5	90.5	91.4	85.7	91.3
2.3	65.6	86.5	95.1	93.9	95.6	96.4	96.7
6	64.0	87.3	97.2	97.8	99.2	96.2	96.8
11.2	41.3	74.5	97.8	98.4	99.0	98.1	98.6

Table 4. *The SE_T of different CNT-PU foam composites at 9 GHz.*

Materials	CNT %	Thickness (mm)	SE_T (dB)	SSE (dB/mm)	SE_A (dB)	Preparation type	β	Ref.
CNT-PU	25 %	2	30.2	15.1	≈ 27	bottom-up	0.60	[23]
CNT-PU	–	20	≈ 35	1.75	≈ 33	dip-coating	–	[27]
CNT decorated hollow glass microspheres- PU	13	10	25.03	2.50	≈ 33.65	bottom-up	0.19	[24]
CNT-PU	9	3.4	≈ 10.5	3.09	≈ 6	bottom-up	0.34	[75]
CNT/PU without buckling structures (UCNPF)	4.35	10	≈ 23	2.3	–	dip-coating	0.53	[76]
single-walled CNT-PU	20	2	≈16	8	–	bottom-up	0.4	[77]
CNT-PU	11.2	2.4	16.2	6.75	13.9	dip-coating	0.60	This work

Table 5. *The comparison of different shielding materials at sub-THz range.*

Composites	Filler %	Thickness (mm)	SE_T (dB)	SSE (dB/mm)	SE_A	Freq	Ref.
MXene/polyelectrolyte (PE)- chitosan (CS) hydrogel	PE content 0.45 g/mL	1	38	38	–	330 GHz	[78]
Cellulose nanofibers (CNF) /sustainable biocarbon (SBC) nanopapers	50 %	3	30	10	29.98 dB	400 GHz	[79]
Graphene/carbon fiber composite aerogels	25 % of CF	4	20	5	96.1 %	330 GHz	[80]
$Ti_3C_2T_x$/poly-(3-glycidoxypropyldimethoxymethylsilane) (PGPDMS) hybrid aerogels	–	1	57.5	57.5	57.4 dB	0.5 – 3 THz	[81]
carbon-coated silicon carbide nanoparticles SiC@C/PDMS	10 % of SiC@C NPs	0.29	12	41.8	–	0.5–3.0 THz	[82]
Epoxy/graphene	1.2 %	1	≈ 12	12	≈ 12 dB	330 GHz	[83]
CNT-PU	11.2	2.4	45.3	18.83	45.2 dB	330 GHz	This work

Figures

Fig. 1. *SEM images of CNT-PU samples, a-b: PU, c-d: 1 wt. % CNT, e-f: 2.3 wt. % CNT, g-h: 6 wt. % CNT, i-j: 11.2 wt. % CNT.*

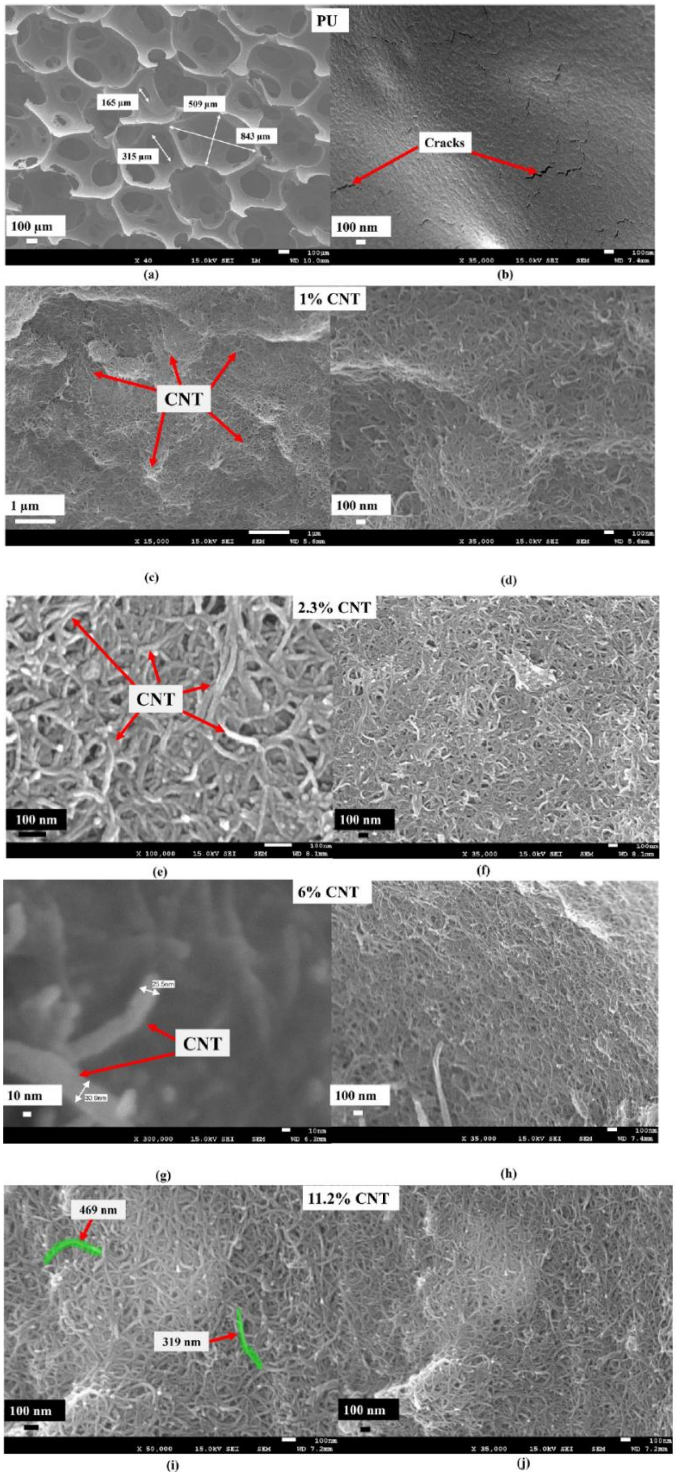

Fig. 2. *Fraction of reflected power of CNT-PU samples in the 5.85 – 330 GHz frequency range.*

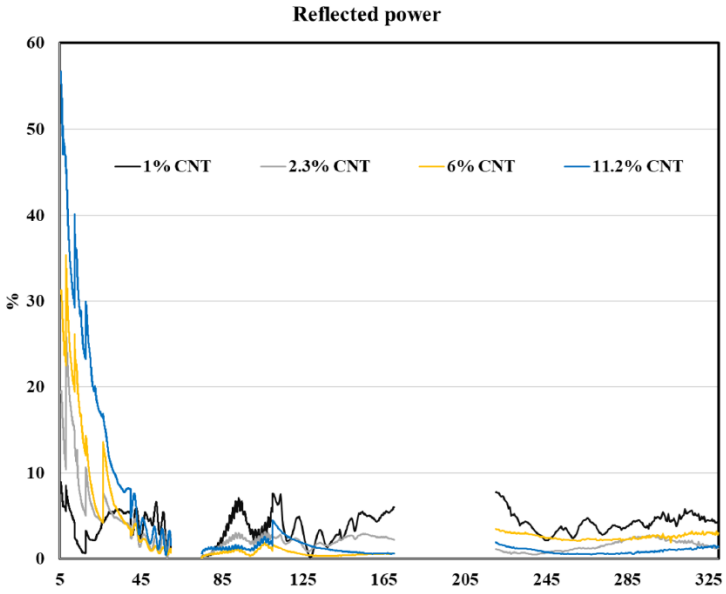

Fig. 3. *Fraction of transmitted power in CNT-PU samples in the 5.85 – 330 GHz frequency range.*

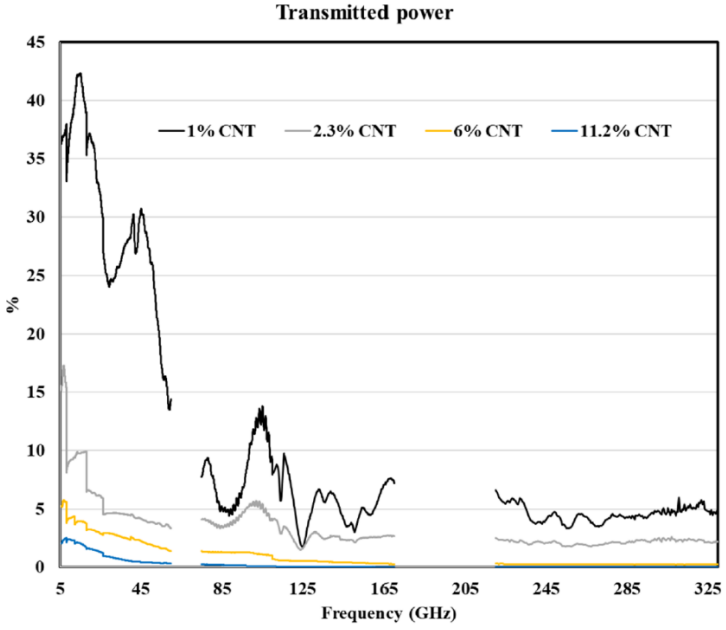

Fig. 4. *Total shielding effectiveness of CNT-PU samples in the 5.85 – 330 GHz frequency range.*

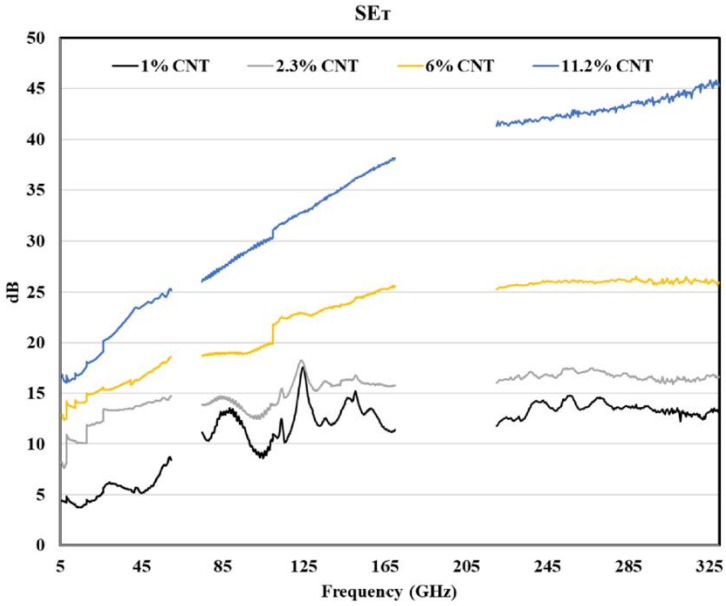

Fig. 5. *Absorption of CNT-PU samples in the 5.85 – 330 GHz frequency range, using Eq. (1).*

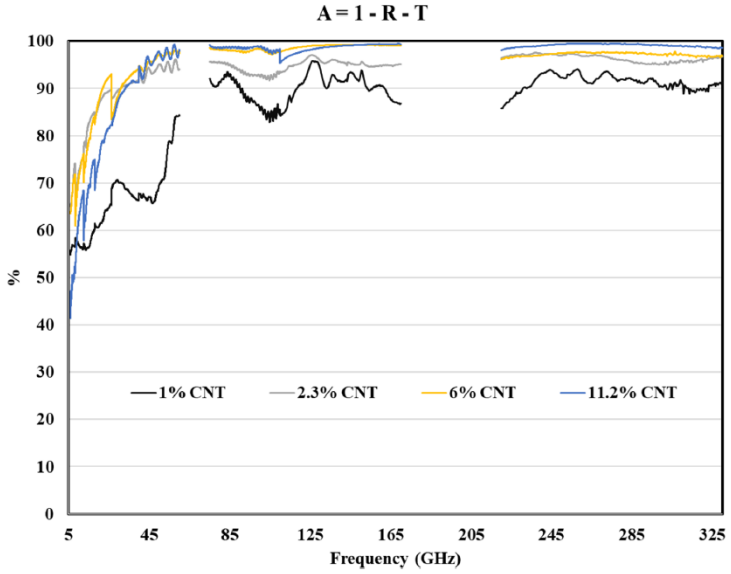

Fig. 6. *SE_R and SE_A contributions to the SE_T of CNT-PU samples at selected frequencies.*

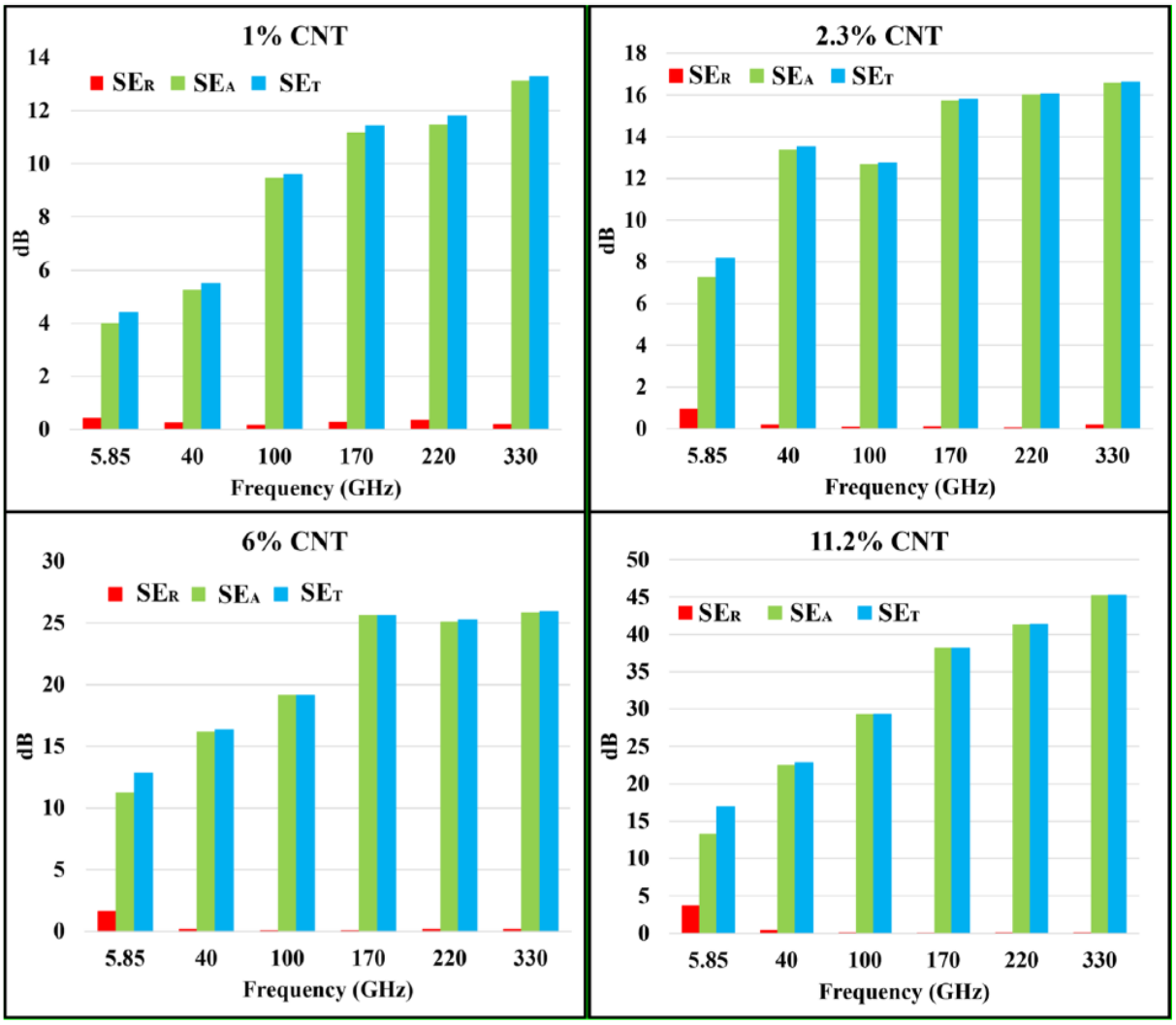

References

(1) *X.-X. Wang, Q. Zheng, Y.-J. Zheng, M.-S. Cao, Green EMI shielding: dielectric/ magnetic "genes" and design philosophy, Carbon. N. Y 206 (2023) 124–141.*

(2) *T.T. Liu, Y.C. Wang, Y.Z. Wang, M.S. Cao, Heterodimensional structure" integrated defect and interface engineering for efficiently EMI shielding and electrochemical response, Adv. Funct. Mater (2024) 2404280.*

(3) *A.A. Isari, A. Ghaffarkhah, S.A. Hashemi, S. Wuttke, M. Arjmand, Structural design for EMI shielding: from underlying mechanisms to common pitfalls, Adv. Mater. 36 (24) (2024) 2310683.*

(4) *Y. Liu, Y. Wang, N. Wu, M. Han, W. Liu, J. Liu, Z. Zeng, Diverse structural design strategies of MXene-based macrostructure for high-performance electromagnetic interference shielding, Nano-Micro. Lett. 15 (1) (2023) 240.*

(5) *J. Kittur, B. Desai, R. Chaudhari, P.K. Loharkar, A comparative study of EMI shielding effectiveness of metals, metal coatings and carbon-based materials, in: IOP Conference Series: Materials Science and Engineering, 2020 012019.*

(6) *N.C. Das, Y. Liu, K. Yang, W. Peng, S. Maiti, H. Wang, Single-walled carbon nanotube/poly (methyl methacrylate) composites for electromagnetic interference shielding, Polym. Eng. Sci. 49 (8) (2009) 1627–1634.*

(7) *Y.-J. Jeon, J.-H. Yun, M.-S. Kang, Analysis of electromagnetic shielding properties of a material developed based on silver-coated copper core-shell spraying, Materials 15 (15) (2022) 5448.*

(8) *J.-M. Thomassin, C. Jérôme, T. Pardoen, C. Bailly, I. Huynen, C. Detrembleur, Polymer/carbon based composites as electromagnetic interference (EMI) shielding materials, Mater. Sci. Eng. 74 (7) (2013) 211–232.*

(9) *J. Kruželák, A. Kvasnčáková, K. Hložeková, I. Hudec, Progress in polymers and polymer composites used as efficient materials for EMI shielding, Nanosc. Adv. 3 (1) (2021) 123–172.*

(10) *J.C. Shu, X. Wan, J.L. Bai, M.Q. Wang, W.Q. Cao, L. Li, M.S. Cao, Controlled modulation of intrinsic electron response in C/CoxTy nanoplates toward multispectral excitation devices, Adv. Mater. 37 (18) (2025) 2501302.*

(11) *B. Lei, C. Zhou, K. Zhang, J. Li, H. Miao, H. Wang, Q. Fan, Z. Yang, G. Wang, Y. Li, Plasma-induced geometry engineering in high-entropy oxide composites for superior electromagnetic absorption, Adv. Funct. Mater 35 (27) (2025) 2425262.*

(12) *T.-T. Liu, L.-Y. Li, P. Gao, L. Li, M.-S. Cao, High-entropy electromagnetic functional materials: from electromagnetic genes to materials design, Mater. Sci. Eng. 164 (2025) 100982.*

(13) *L.H. Yao, J.C. Shu, J.G. Zhao, J.Y. Zong, M.S. Cao, W.Q. Cao, Heterodimensional structure integrating electromagnetic functions and hybrid energy storage to drive multifunctional devices, Adv. Funct. Mater 35 (31) (2025) 2503307.*

(14) *L. Zhang, M. Liu, S. Roy, E.K. Chu, K.Y. See, X. Hu, Phthalonitrile-based carbon foam with high specific mechanical strength and superior electromagnetic interference shielding performance, ACS. Appl. Mater. Interfaces 8 (11) (2016) 7422–7430.*

(15) *M. Ates, S. Karadag, A.A. Eker, B. Eker, Polyurethane foam materials and their industrial applications, Polym. Int 71 (10) (2022) 1157–1163.*

(16) *A. Barick, D. Tripathy, Preparation and characterization of carbon nanofiber reinforced thermoplastic polyurethane nanocomposites, J. Appl. Polym. Sci 124 (1) 765–780.*

(17) *T. Gupta, B.P. Singh, S. Teotia, V. Katyal, S. Dhakate, R. Mathur, Designing of multiwalled carbon nanotubes reinforced polyurethane composites as electromagnetic interference shielding materials, J. Polym. Res. 20 (2013) 1–7.*

(18) *A.S. Hoang, Electrical conductivity and electromagnetic interference shielding characteristics of multiwalled carbon nanotube filled polyurethane composite films, Adv. Natur. Sci. 2 (2) (2011) 025007.*

(19) *S.D. Ramôa, G.M. Barra, R.V. Oliveira, M.G. de Oliveira, M. Cossa, B.G. Soares, Electrical, rheological and electromagnetic interference shielding properties of thermoplastic polyurethane/carbon nanotube composites, Polym. Int 62 (10) 1477–1484.*

(20) *G. Sang, P. Xu, C. Liu, P. Wang, X. Hu, Y. Ding, Synergetic effect of Ni@ MWCNTs and hybrid MWCNTs on electromagnetic interference shielding performances of polyurethane–matrix composite foams, Ind. Eng. Chem. Res 59 (34) (2020) 15233–15241.*

(21) *R. Olejník, S. Goňa, P. Slobodian, J. Matáš , R. Moučka, R. Daňová, Polyurethane-carbon nanotubes composite dual band antenna for wearable applications, Polymers. (Basel) 12 (11) (2020) 2759.*

(22) *M.I. Hussein, S.S. Jehangir, I. Rajmohan, Y. Haik, T. Abdulrehman, Q. Clément, N. Vukadinovic, Microwave absorbing properties of metal functionalized-CNT- polymer composite for stealth applications, Sci. Rep 10 (1) (2020) 16013.*

(23) *G. Sang, P. Xu, T. Yan, V. Murugadoss, N. Naik, Y. Ding, Z. Guo, Interface engineered microcellular magnetic conductive polyurethane nanocomposite foams for electromagnetic interference shielding, Nano-Micro. Lett. 13 (2021) 1–16.*

(24) *S. Sultana, M. Rahaman, M.R. Chandan, Enhancing EMI shielding efficiency of polyurethane foam by incorporating MWCNT-decorated hollow glass microspheres, ACS. omega 10 (2) (2025).*

(25) *A.R. Boccaccini, F. Chicatun, J. Cho, O. Bretcanu, J.A. Roether, S. Novak, Q. Chen, Carbon nanotube coatings on bioglass-based tissue engineering scaffolds, Adv. Funct. Mater 17 (15) (2007) 2815–2822.*

(26) *K. Nakagawa, Foam materials made from carbon nanotubes, Carbon. Nanotubes- From. Res. Appl. (2011).*

(27) *Y. Luo, Y. Guo, C. Wei, J. Chen, G. Zhao, Q. Yuan, Y. Zhu, Lightweight, compressible, and stretchable composite foams for ultra-efficient and high-stable electromagnetic interference shielding materials, Carbon. N. Y 215 (2023) 118480.*

(28) *A. Tanaka, K. Arita, C. Kobayashi, T. Nishiwaki, T. Tanabe, S. Fujii, Fundamental properties of Sub-THz reflected waves for water content estimation of reinforced concrete structures, Buildings 14 (4) (2024) 1076.*

(29) *C. Chen, W. Zhao, H. Zhang, T. Hauffman, Z. Zhang, J. Stiens, Improvement of absorbing stability of carbon nanofibers in sub-terahertz domain using the surface modification of zinc oxide, Ceram. Int 49 (11) (2023) 18491–18501.*

(30) *B. Park, S. Hwang, H. Lee, Y. Jung, T. Kim, S.J. Kwon, D. Jung, S.b. Lee, Absorption-dominant electromagnetic interference (EMI) shielding across multiple mmWave bands using conductive patterned magnetic composite and double- walled carbon nanotube film, Adv. Funct. Mater 34 (40) (2024) 2406197.*

(31) *Huynen, Investigation of microwave absorption mechanisms in microcellular foamed conductive composites, Micro 1 (1) (2021) 86–101.*

(32) *S. Venkatachalam, K. Zeranska-Chudek, M. Zdrojek, D. Hourlier, Carbon-based terahertz absorbers: materials, applications, and perspectives, Nano. Select 1 (5) (2020) 471–490.*

(33) *S.F. Mahmoud, A.R. AlAjmi, Analysis and design of carbon nanotube antenna in the subterahertz frequency range, in: 2014 Loughborough Antennas and Propagation Conference (LAPC), 2014, pp. 206–209.*

(34) *S. Puthukodan, E. Dadrasnia, V. Vinod, H.Lamela Rivera, G. Ducournau, J. F. Lampin, Optical properties of carbon nanotube thin films in subterahertz frequency regime, Microw. Opt. Technol. Lett 56 (8) (2014) 1895–1898.*

(35) *S. Smirnov, A. Przewłoka, A. Krajewska, D. Zykov, P. Demchenko, J. Oberhammer, M. Khodzitsky, I. Nefedov, D. Lioubtchenko, Sub-THz phase shifters enabled by photoconductive single-walled carbon nanotube layers, Adv. Photon. Res. 4 (4) (2023) 2200042.*

(36) *D. Suzuki, Y. Takida, Y. Kawano, H. Minamide, N. Terasaki, Carbon nanotube-based, serially connected terahertz sensor with enhanced thermal and optical efficiencies, Sci. Technol. Adv. Mater 23 (1) (2022) 424–433.*

(37) *Z. Barani, K. Stelmaszczyk, F. Kargar, Y. Yashchyshyn, G. Cywiński, S. Rumyantsev, A.A. Balandin, Efficient terahertz radiation absorption by dilute graphene composites, Appl. Phys. Lett 120 (6) (2022).*

(38) *V.D. Moskalenko, T.N. Shematilo, K.V. Dorozhkin, A.V. Badin, Sub-THz absorbers based on BaTiO3/epoxy composites, J. Phys. (2021) 012034.*

(39) *K. Zeranska-Chudek, A. Siemion, N. Palka, A. Mdarhri, I. Elaboudi, C. Brosseau, M. Zdrojek, Terahertz shielding properties of carbon black based polymer nanocomposites, Materials. (Basel) 14 (4) (2021) 835.*

(40) *Z. Huang, H. Chen, S. Xu, L.Y. Chen, Y. Huang, Z. Ge, W. Ma, J. Liang, F. Fan, S. Chang, Graphene-based composites combining both excellent terahertz shielding and stealth performance, Adv. Opt. Mater 6 (23) (2018) 1801165.*

(41) *Z. Barani, F. Kargar, K. Godziszewski, A. Rehman, Y. Yashchyshyn, S. Rumyantsev, G. Cywiński, W. Knap, A.A. Balandin, Graphene epoxy-based composites as efficient electromagnetic absorbers in the extremely high-frequency band, ACS. Appl. Mater. Interfaces 12 (25) (2020) 28635–28644.*

(42) *S. Myllymaki, M. Teirikangas, M. Kokkonen, BaSrTiO3 ceramic-polymer composite¨ material lens antennas at 220–330 GHz telecommunication applications, Electron. Lett 56 (22) (2020) 1165–1167.*

(43) *A. Aqel, K.M. Abou El-Nour, R.A. Ammar, A. Al-Warthan, Carbon nanotubes, science and technology part (I) structure, synthesis and characterisation, Arab. J. Chem. 5 (1) (2012) 1–23.*

(44) *I. Molenberg, M.M. Bernal, P. Bollen, D. Spote, R. Verdejo, T. Pardoen, C. Bailly, I. Huynen, Simple, convenient, and nondestructive electromagnetic characterization technique for composite and multiscale hybrid samples at microwave frequencies, Microw. Opt. Technol. Lett 56 (2) (2014) 504–509.*

(45) *G.F. Engen, C.A. Hoer, Thru-reflect-line: an improved technique for calibrating the dual six-port automatic network analyzer, IEEE. Trans. Microwave. Theory. Tech 27 (12) (1979) 987–993.*

(46) *A. Sotiropoulos, S. Koulouridis, A. Masouras, V. Kostopoulos, H.T. Anastassiu, Carbon nanotubes films in glass fiber polymer matrix forming structures with high absorption and shielding performance in X-band, Compos. Part. B 217 (2021) 108896.*

(47) *Y. Bhattacharjee, I. Arief, S. Bose, Recent trends in multi-layered architectures towards screening electromagnetic radiation: challenges and perspectives, J. Mater. Chem. C 5 (30) (2017) 7390–7403.*

(48) *M.-S. Cao, W.-L. Song, Z.-L. Hou, B. Wen, J. Yuan, The effects of temperature and frequency on the dielectric properties, electromagnetic interference shielding and microwave-absorption of short carbon fiber/silica composites, Carbon. N. Y 48 (3) (2010) 788–796.*

(49) *H.-Z. Ma, J.-N. Zhao, R. Tang, Y. Shao, K. Ke, K. Zhang, B. Yin, M.-B. Yang, Polypyrrole@ CNT@ PU conductive sponge-based triboelectric nanogenerators for Human motion monitoring and self-powered Ammonia sensing, ACS. Appl. Mater. Interfaces 15 (47) (2023) 54986–54995.*

(50) *W. Chen, W. Duan, Y. Liu, Q. Wang, F. Qi, Facile fabrication of multifunctional polymer composites based on three-dimensional interconnected networks of graphene and carbon nanotubes, Ind. Eng. Chem. Res 58 (47) (2019) 21531–21541.*

(51) *L. Huang, J. Chen, Y. Xu, D. Hu, X. Cui, D. Shi, Y. Zhu, Three-dimensional light- weight piezoresistive sensors based on conductive polyurethane sponges coated with hybrid CNT/CB nanoparticles, Appl. Surf. Sci 548 (2021) 149268.*

(52) *D. Lee, S.G. Kim, J. Kim, N. Kim, K.-H. Ryu, D.-Y. Kim, N.D. Kim, J.Y. Hwang, Y. Piao, S. An, Highly conductive and mechanically strong metal-free carbon nanotube composite fibers with self-doped polyaniline, Carbon. N. Y 213 (2023) 118308.*

(53) *X. Liang, Y. Shen, Y. Liu, J. Wang, Y. Gao, S. Li, M. Wang, S. Gao, Investigations on the basic electrical properties of polyurethane foam material, in: IEEE 11th International Conference on the Properties and Applications of Dielectric Materials (ICPADM), 2015, pp. 863–866. Sydney, NSW, Australia.*

(54) *S. Bi, Y.-Z. Song, G.-L. Hou, H. Li, Z.-H. Liu, Z.-L. Hou, J. Zhang, Sandwich nanoarchitectonics of heterogenous CB/CNTs honeycomb composite for impedance matching design and microwave absorption, J. Alloys. Compd 943 (2023) 169154.*

(55) *H. Li, S. Bi, J. Cai, X. Chu, G. Hou, J. Zhang, T. Wu, Reduced graphene oxide/ nonwoven fabric filled honeycomb composite structure for broadband microwave absorption, Carbon. N. Y 223 (2024) 119005.*

(56) *M.S. Cao, X.X. Wang, M. Zhang, W.Q. Cao, X.Y. Fang, J. Yuan, Variable- temperature electron transport and dipole polarization turning flexible multifunctional microsensor beyond electrical and optical energy, Adv. Mater. 32 (10) (2020) 1907156.*

(57) *X. He, J. Zhou, L. Jin, X. Long, H. Wu, L. Xu, Y. Gong, W. Zhou, Improved dielectric properties of thermoplastic polyurethane elastomer filled with core–shell structured PDA@ TiC particles, Materials. (Basel) 13 (15) (2020) 3341.*

(58) *A. Saib, L. Bednarz, R. Daussin, C. Bailly, X. Lou, J.-M. Thomassin, C. Pagnoulle, C. Detrembleur, R. Jérôme, I. Huynen, Carbon nanotube composites for broadband microwave absorbing materials, IEEE. Trans. Microwave. Theory. Tech 54 (6) (2006) 2745–2754.*

(59) *B. Wen, M.-S. Cao, Z.-L. Hou, W.-L. Song, L. Zhang, M.-M. Lu, H.-B. Jin, X.-Y. Fang, W.-Z. Wang, J. Yuan, Temperature dependent microwave attenuation behavior for carbon-nanotube/silica composites, Carbon. N. Y 65 (2013) 124–139.*

(60) *S. Gong, Z.H. Zhu, M. Arjmand, U. Sundararaj, J.T. Yeow, W. Zheng, Effect of carbon nanotubes on electromagnetic interference shielding of carbon fiber reinforced polymer composites, Polym. Compos 39 (S2) (2018) E655–E663.*

(61) *D. Chung, A perspective on electromagnetic interference shielding materials comprising exfoliated graphite, Carbon. N. Y 216 (2024) 118569.*

(62) *S.M. Wentworth, M.E. Baginski, D.L. Faircloth, S.M. Rao, L.S. Riggs, Calculating effective skin depth for thin conductive sheets, in: 2006 IEEE Antennas and Propagation Society International Symposium, 2006, pp. 4845–4848.*

(63) *J. Chen, Z. Pei, B. Chai, P. Jiang, L. Ma, L. Zhu, X. Huang, Engineering the dielectric constants of polymers: from molecular to mesoscopic scales, Adv. Mater. 36 (52) (2024) 2308670.*

(64) *K.C. Kao, Dielectric Phenomena in Solids, Elsevier, 2004.*

(65) *S. Singh, A. Kaur, P. Kaur, L. Singh, High-temperature dielectric relaxation and electric conduction mechanisms in a LaCoO3-modified Na0. 5Bi0. 5TiO3 system, ACS. Omega 8 (28) (2023) 25623–25638.*

(66) *H.J. Salacinski, M. Odlyha, G. Hamilton, A.M. Seifalian, Thermo-mechanical analysis of a compliant poly (carbonate-urea) urethane after exposure to hydrolytic, oxidative, peroxidative and biological solutions, Biomaterials 23 (10) (2002) 2231–2240.*

(67) *T. Pluta, G. Skrzynski, Time-dependent DFT calculations of the dipole moment and´ polarizability for excited states. Adv Quantum Chem, Elsevier, 2021, pp. 305–327.*

(68) *R.K. Mahmoud, M. Taha, A. Zaher, and R.M. Amin, "Selective and highly efficient adsorption of a mixture of anionic and cationic dyes as synthetic wastewater absorbents on layered double hydroxide: experimental and computational studies," 2021.*

(69) *X. Gao, X. Wang, J. Cai, Y. Zhang, J. Zhang, S. Bi, Z.-L. Hou, CNT cluster arrays grown on carbon fiber for excellent green EMI shielding and microwave absorbing, Carbon. N. Y 211 (2023) 118083.*

(70) *A.P. Singh, M. Mishra, A. Chandra, S. Dhawan, Graphene oxide/ferrofluid/cement composites for electromagnetic interference shieldingapplication, Nanotechnology 22 (46) (2011) 465701.*

(71) *T. Guo, X. Chen, L. Su, C. Li, X. Huang, X.-Z. Tang, Stretched graphene nanosheets formed the "obstacle walls" in melamine sponge towards effective electromagnetic interference shielding applications, Mater. Des 182 (2019) 108029.*

(72) *M.B. Hasani, K. Inamdar, P. Bhale, Effect of thickness and conductivity on electromagnetic interference shielding effectiveness of Bio composite shields, in: 2024 S International Conference on Microwave, Antenna and Communication (MAC), 2024, pp. 1–6.*

(73) *Y. Si, S. Shi, J. Hu, Applications of electrospinning in human health: from detection, protection, regulation to reconstruction, Nano. Today 48 (2023) 101723.*

(74) *S. Manobalan, S. Bose, T. Sumangala, Effect of thickness on the EMI shielding effectiveness of epoxy composites with cobalt ferrite and graphene, Mater. Today 90 (2023) 128–132.*

(75) *Z. Lei, D. Tian, X. Liu, J. Wei, K. Rajavel, T. Zhao, Y. Hu, P. Zhu, R. Sun, C.- P. Wong, Electrically conductive gradient structure design of thermoplastic polyurethane composite foams for efficient*

electromagnetic interference shielding and ultra-low microwave reflectivity, Chem. Eng. J. 424 (2021) 130365.

(76) K. Huang, M. Chen, G. He, X. Hu, W. He, X. Zhou, Y. Huang, Z. Liu, Stretchable microwave absorbing and electromagnetic interference shielding foam with hierarchical buckling induced by solvent swelling, Carbon. N. Y 157 (2020) 466–477.

(77) Z. Liu, G. Bai, Y. Huang, Y. Ma, F. Du, F. Li, T. Guo, Y. Chen, Reflection and absorption contributions to the electromagnetic interference shielding of single- walled carbon nanotube/polyurethane composites, Carbon. N. Y 45 (4) (2007) 821–827.

(78) W. Ouyang, L. Mei, Q. Liu, C. Ding, Y. Liu, C. Zhao, L. Xu, F. Lu, D. Luo, C. Miao, Ultrathin-flexible multifunctional MXene composite hydrogels with good mechanical properties-high strain sensitivity and ultra-broadband EMI shielding performances, Chem. Eng. J. 494 (2024) 153068.

(79) A.R. Pai, Y. Lu, S. Joseph, N.M. Santhosh, R. Degl'Innocenti, H. Lin, R. Letizia, C. Paoloni, S. Thomas, Ultra-broadband shielding of cellulose nanofiber commingled biocarbon functional constructs: a paradigm shift towards sustainable terahertz absorbers, Chem. Eng. J. 467 (2023) 143213.

(80) Y. Cao, Z. Cheng, R. Wang, X. Liu, T. Zhang, F. Fan, Y. Huang, Multifunctional graphene/carbon fiber aerogels toward compatible electromagnetic wave absorption and shielding in gigahertz and terahertz bands with optimized radar cross section, Carbon. N. Y 199 (2022) 333–346.

(81) Q. Xie, Y. Zhao, D. Liang, L. Zhang, Q. Wen, F. Tang, M. Hu, L. Deng, P. Zhou, Lightweight MXene-based hybrid aerogels with ultrabroadband terahertz absorption and anisotropic strain sensitivity, ACS. Appl. Mater. Interfaces 14 (51) (2022) 57008–57015.

(82) F. Huang, S. Fan, Y. Tian, X. Qu, X. Li, M. Javid, X. Zhang, Z. Zhang, X. Dong, T. Cao, Thermally stable carbon-coated SiC/polydimethylsiloxane nanocomposites for EMI shielding in the terahertz range, Mater. Res. Bull 153 (2022) 111900.

(83) Z. Barani, K. Stelmaszczyk, F. Kargar, Y. Yashchyshyn, G. Cywiński, S. Rumyantsev, and A.A. Balandin, "Efficient absorption of terahertz radiation in graphene polymer composites," arXiv preprint arXiv:2109.01082, 2021.